Journal of the Korean Crystal Growth and Crystal Technology
Vol. 33, No. 1 (2023) 37-44
https://doi.org/10.6111/JKCGCT.2023.33.1.037

p-ISSN 1225-1429
e-ISSN 2234-5078

Oxygen reduction reaction and electrochemical properties of transition metal doped (Pr,Ba)$Co_2O_{5+\delta}$

Kanghee Jo and Heesoo Lee†

School of Materials Science and Engineering, Pusan National University, Busan 46241, Korea

(Received January 4, 2023)
(Revised January 30, 2023)
(Accepted February 2, 2023)

Abstract Transition metal (Me = Cu, Fe, Ni) doped (Pr, Ba)$Co_2O_{5+\delta}$ (PBCO) material were investigated in terms of electronic structure change and electrochemical properties. It was confirmed that (Pr, Ba)(Co, Cu)$O_{5+\delta}$ (PBCCu) and (Pr, Ba)(Co, Fe)$O_{5+\delta}$ (PBCFe) showed cubic and orthorhombic structures, respectively, but (Pr, Ba)(Co, Ni)$O_{5+\delta}$ (PBCNi) showed secondary phases. PBCCu has an average particle diameter of 1093 nm, and PBCO and PBCFe have an average particle diameter of 495.1 nm and 728 nm, respectively. The average oxidation values of B site ions in PBCMe were calculated to be 3.26 (PBCO), 2.48 (PBCCu), 3.32 (PBCFe), and valence band maximum (VBM) was −0.42 eV (PBCO), −0.58 eV (PBCCu), −0.11 eV (PBCFe). It is expected that PBCCu easily interacts with adsorbed oxygen due to the lowest oxidation value and the highest VBM. The polarization resistance was 0.91 Ω cm^2 (PBCO), 0.77 Ω cm^2 (PBCCu), 1.06 Ω cm^2 (PBCFe) at 600°C, showing the lowest polarization resistance of PBCCu.

Key words Transition metal doped (Pr, Ba)$Co_2O_{5+\delta}$, Oxygen vacancy formation, Valence band structure, Oxygen reduction reaction

1. Introduction

Solid oxide fuel cells (SOFC) are devices that produces electrical energy from chemical energy and is widely studied as a next-generation energy technology. In particular, among various fuel cells, SOFC operating at relatively high temperature (500~1000°C) can achieve high energy conversion efficiency of over 80 % without using noble metal catalysts such as Pt, Ir, Pd, Au. SOFC can be widely used from small fuel cells for transportation equipment to large-capacity generators for power plants [1,2].

For an efficient SOFC cathode, high catalytic activity for oxygen reduction reactions (ORR) at a temperature of 400 to 600°C is essential [3]. This temperature is lower than the existing operating temperature, which can reduce material deterioration, improve structural stability and ease of sealing. However, one of the important obstacles acting on lowering the operating temperature is a high polarization resistance due to the sluggish reaction rate of the material [4,5].

Perovskite oxide (ABO_3) is an electrocatalyst material widely used and studied as a material for SOFC cathode. Perovskite material has mixed conductivity through composition control, so that reaction occurs on the entire cathode surface. In addition, forming a nano-sized catalyst on the surface through infiltration and exsolution have been studied to obtain higher efficiency [6-8]. When the A-site of perovskite oxide is doped with a metal ion A′ (alkali rare-earth metal ion) having a large atomic radius difference, cation ordering occurs, and a layered perovskite oxide structure is formed. Recently, double perovskite oxide ($AA'B_2O_{5+\delta}$) has been widely studied due to its excellent electronic conductivity and oxygen ion transport characteristics induced by its special crystal structure [9]. Among them, (Ln, Ba)$Co_2O_{5+\delta}$ (Ln = Pr, Sm, Gd, etc.) based layered perovskite oxides are in the spotlight as core materials for IT-SOFC [10,11]. In particular, the layered structure of [LnO_x]-[CoO_2]-[BaO]-[CoO_2]-[LnO_x] appears repeatedly, forming an oxygen diffusion pathway and reducing the binding strength with oxygen, and contribute to the improvement of the ORR activity [12].

The electrical properties of perovskite and layered perovskite oxides are greatly influenced by the B-site transition metal ion, which is highly dependent on the electronic structure including the valence band structure. Various studies have suggested e_g orbital filling of B-site ion, O p-band center, and charge transfer energy as indicators for predicting the performance in terms of ORR and OER catalysts [13]. Lee et al., focusing on the

†Corresponding author
E-mail: heesoo@pusan.ac.kr

importance of oxygen conduction, predicted the ORR catalytic activity of SOFC by comparing the O p-band center with measurable indicators such as polarization resistance and surface exchange constant [14,15]. Zhu et al. studied the relationship between polarization resistance and structure of valence band composed of O 2p band and Co3d band of LSCO thin film [16].

In this study, various transition metal elements (Me = Cu, Fe, Ni) were doped into (Pr, Ba)$Co_2O_{5+\delta}$ to improve the electrochemical properties. Crystal structure and powder characterization was performed to analyze the phase formation and specific surface area, particle size distribution for the layered perovskite doped with each element. The change in the electronic structure according to the doped transition metal ions was analyzed with X-ray photoelectron spectroscopy (XPS) and the relationship with the electrochemical properties was studied. Based on these results, transition metals with the better properties were selected and the mechanisms for improving the electrochemical properties were investigated for more diverse compositions to find the optimum composition.

2. Experimental Procedures

The (Pr, Ba)(Co, Me)$O_{5+\delta}$ (PBCMe, Me = Cu, Fe, Ni) nanopowders were synthesized via EDTA-Citric acid Complex Process (ECCP). Praseodymium nitrate hexahydrate ($Pr(NO_3)_3 \cdot 6H_2O$, Sigma-Aldrich), barium nitrate ($Ba(NO_3)_2$), Alfa Aesar), cobalt nitrate tetrahydrate ($Co(NO_3)_3 \cdot 6H_2O$, Sigma-Aldrich), copper nitrate hemipentahydrate ($Cu(NO_3)_2 \cdot 2.5H_2O$, Sigma-Aldrich), iron nitrate nonahydrate ($Fe(NO_3)_3 \cdot 9H_2O$) and nickel nitrate ($Ni(NO_3)_2 \cdot 6H_2O$) were used as metal precursors. EDTA powder (Alfa Aesar) and crystallized citric acid (Samchun Chemical), both with purities greater than 99.5 %, served as chelating agents. The required amounts of the analytic precursors according to composition stoichiometry, Pr:Ba:Co:Me = 1:1:1:1, were dissolved in distilled water with stirring to prepare homogeneous metal nitrate solutions.

The required amounts of analytic reagents according to the stoichiometry of the composite were dissolved in deionized water with stirring to prepare a homogeneous metal nitrate solution. EDTA-NH_4OH and citric acid were added to the solution in sequence at a mole ratio of total metal ions: EDTA: citric acid of 1:1:2. The solution was heated at 80°C continuously with stirring to facilitate water evaporation while adjusting pH to 10. A clear viscous gel was finally obtained under stirring and heating, which was solidified by pre-heating at 250°C for several hours. The solidified precursors were calcined in air at 950°C for 2 hours.

The electrolyte disc was fabricated by uniaxial pressing of commercial Sm-doped Ceria powders (SDC, FuelCellMaterials) into a 20 Φ disk mold at 3.2 metric ton and sintered at 1500°C for 5 hours. And the SDC pellet was polished to 0.5 mm thickness. The synthesized cathode powders were mixed with a binder prepared from α-terpineol and ethyl-cellulose to form cathode pastes. The PBCMe cathode pastes were screen-printed on to both sides of the SDC pellets with an area of 1.13 cm^2 to form symmetric cell structures. The symmetric cells were sintered at 900°C for 2 hours in air. Pt current collectors were brushed on both sides of the symmetric cells, and Pt meshes connected with Pt wires were attached to each electrode.

Crystal structure analysis was conducted with an X-ray diffractometer. Powder X-ray diffraction (XRD, Ultima IV, Rigaku) of the cathode powders was performed at room temperature using a step scan procedure (0.008°/2θ, 4 s per step) over a 2θ range of 20~80° using a Cu Kα (wavelength: 0.1543 nm) source.

Powder morphology was performed using a field-emission scanning electron microscope (FE-SEM, MIRA3, TESCAN). Specific surface area was measured according to KS L ISO 18757 standard. Particle size distribution was measured using a Mastersizer (Malvern Mastersizer 3000, Malvern Instrument, UK).

The Me doped (Pr, Ba)$Co_2O_{5+\delta}$ surface was characterized by XPS using Al Kα radiation (hν = 1486.6 eV) upon increasing the temperature in ultra-high vacuum condition.

The electrical conductivity of the cathodes was measured using a four-probe direct current conductivity technique over a 300~950°C temperature range. The distance of Pt wires was 10 mm. Direct current of 50 mA was supplied to them by a current source (Keithley 2400, Solon, Ohio USA), and the corresponding voltage drops were collected using a multimeter (Agilent, 34401A, Santa Clara, California USA). The electrical conductivity was calculated by following formula.

$$\sigma = \frac{L}{R \times A} = \frac{I \times L}{V \times A}$$

, where σ is conductivity, R is resistance, V is measured voltage, I is current, L is distance between voltage-sensing electrodes, and A is area of measured sample.

Impedance measurements were carried out using an IviumStat (Ivium, Netherlands) instrument over the frequency range from 10^6 to 0.01 Hz with a 10 mV excitation voltage at operating temperatures of 600~900°C in air. The impedance measurements were acquired under an open circuit condition. The electrochemical impedance spectra (EIS) results were multiplied by 0.5 to account for the two electrodes. The measured impedance data were plotted on the complex plane.

3. Results and Discussion

The phase formation of the (Pr, Ba)(Co, Me)$O_{5+\delta}$ (PBCMe) was analyzed through XRD. The basic composition, (Pr, Ba)$Co_2O_{5+\delta}$ (PBCO), showed pure orthorhombic structure and all peaks are indexed according to the *Pmmm* structure. As shown in Fig. 1, PBCCu showed pseudo-cubic structure and PBCFe showed pure tetragonal structure and on the other hand, when Ni was doped into PBCO, NiO and $PrBaO_3$ were formed as a secondary phase. It was confirmed that PBCO was easily doped with Fe and Co to form a stable phase, but Ni was not easily doped and formed a secondary phase [17].

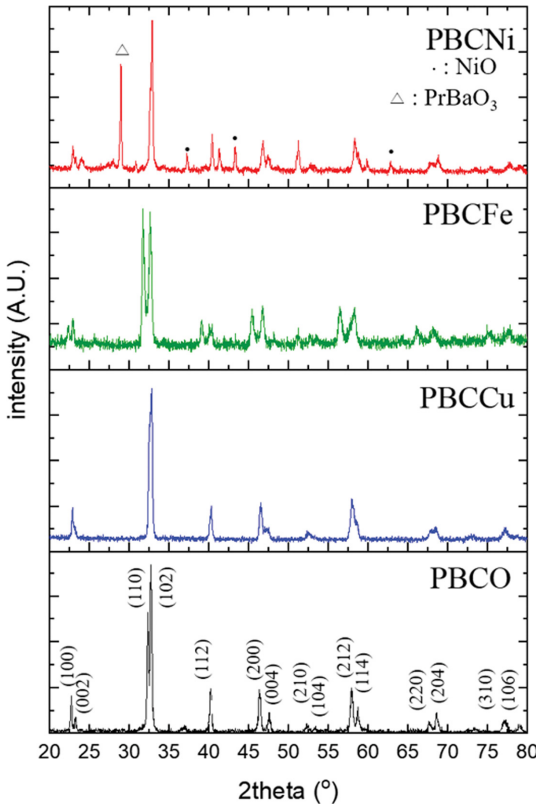

Fig. 1. X-ray diffraction patterns of PBCMe.

Spherical powder was observed in all compositions through SEM as shown in Fig. 2. In the case of PBCNi, it was confirmed that needle-shaped secondary phase was formed in the spherical particles. Table 1 shows the powder characteristics of the $PrBaCoMeO_{5+\delta}$ (PBCMe) powders calcined at 950°C. PBCO showed the particle size of 495.1 nm, 1093 nm for PBCCu, 728 nm for PBCFe and 408.2 nm for PBCNi which indicates that Cu and Fe lowered the melting temperature of the powder and contributed to the coarsening and particle growth [18,19].

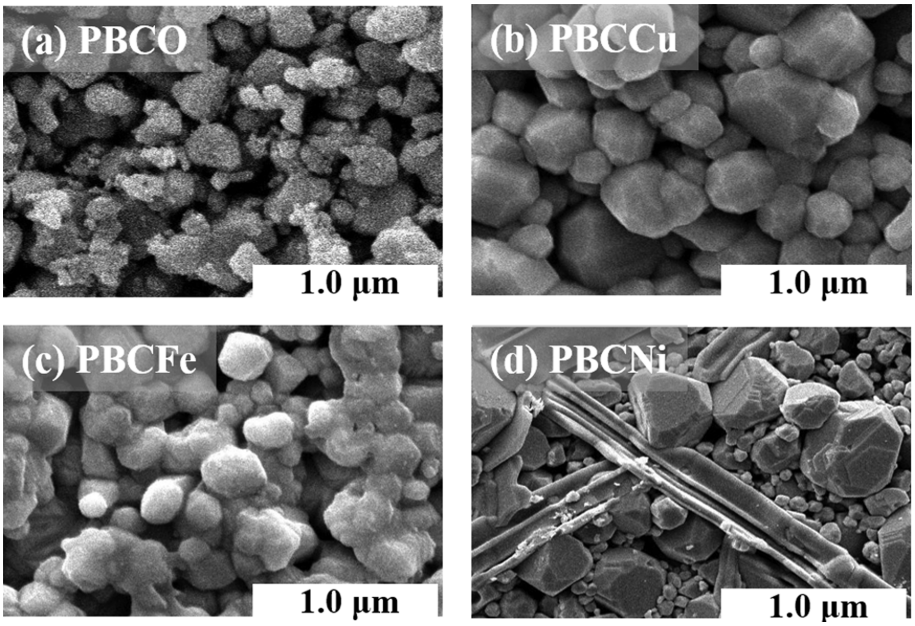

Fig. 2. Powder morphology of sample powders (a) PBCO, (b) PBCCu, (c) PBCFe, (d) PBCNi.

Table 1
Powder characteristics of Me doped $PrBaCo_2O_{5+\delta}$

Sample name	Average particle size (nm)	Specific surface area (m^2/g)
PBCO	495.1	2.1233
PBCFe	728	1.6994
PBCNi	408.2	2.6808
PBCCu	1093	0.3621

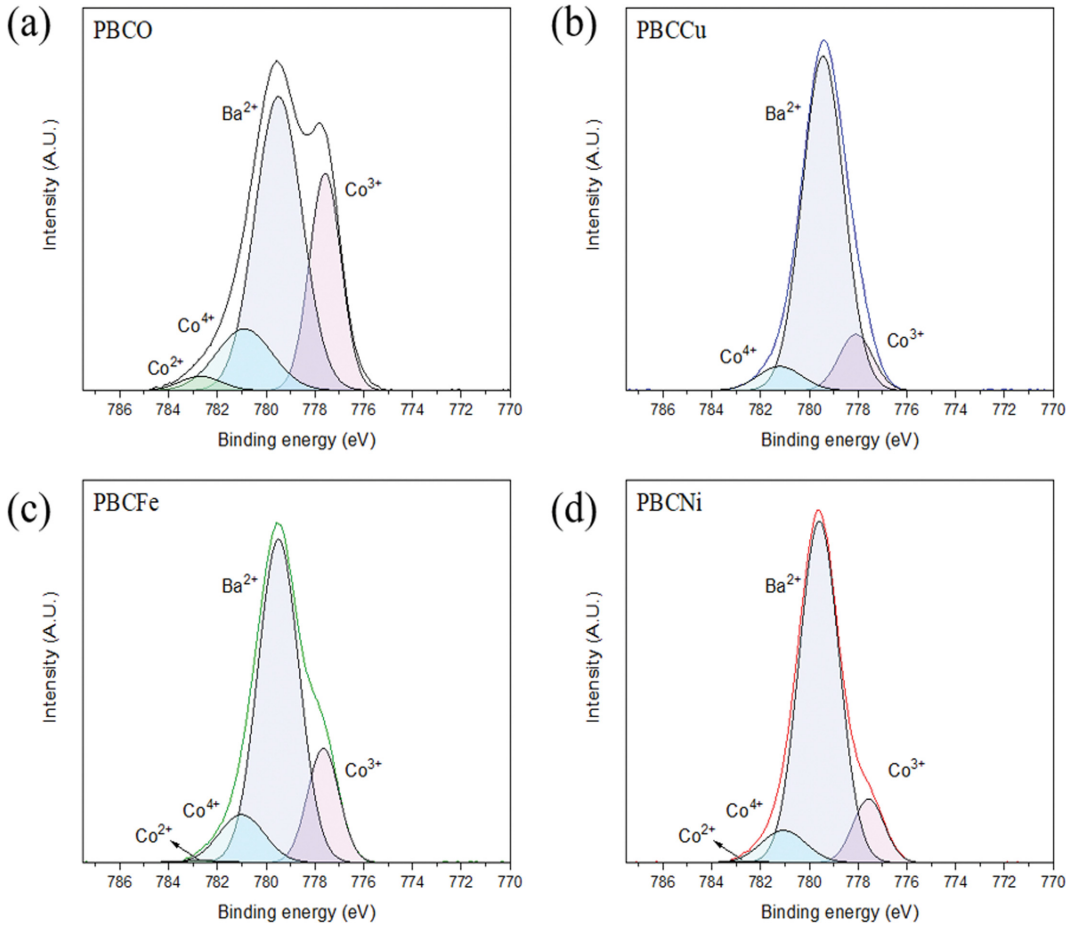

Fig. 3. Ba $3d_{5/2}$ and Co $2p_{3/2}$ core level spectra (solid line) and the fit results (colored area) (a) PBCO, (b) PBCCu, (c) PBCFe and (d) PBCNi.

As the specific surface area was the opposite trend, PBCNi showed the largest specific surface area of 2.6808 m^2/g and PBCCu showed the smallest specific surface area of 0.3621 m^2/g.

Figures 3 and 4 show the XPS core level spectra of B site metal ions of $PrBaCoMeO_{5+\delta}$ (Me = Cu, Fe, Ni), respectively. In Fig. 3, the core level spectra of Co $2p_{3/2}$ and Ba $3d_{5/2}$ were observed at 785~790 eV, and the weak satellite shake up peak caused by Co ions appeared at 785 eV to 790 eV [17,20-22]. Figure 4(a) shows the core level spectra of Cu $2p_{3/2}$ and Pr $3d_{5/2}$ is observed at 920 eV to 945 eV [23,24]. In addition, a weak satellite shake-up peak due to Cu was observed. Figure 4(b) shows the Fe $2p_{3/2}$ core level spectra from 705 eV to 720 eV [25]. And Fig. 4(c) shows the Ni $2p_{3/2}$ core level spectra observed at 850 eV to 865 eV and the satellite shake-up peak due to Ni ions [26].

When PBCO is doped with a transition metal, the Co ions are substituted with the transition metal ions, and the average oxidation number of the B site metal ions changes. In the layered perovskite, the average oxidation number of B site metal ions is inversely proportional to the number of lattice oxygen vacancy as shown in Table 2. In the case of PBCCu, because Cu ions have only 1+ and 2+ as oxidation states unlike other elements, Cu ions completely subsitute Co^{2+} and reduce the

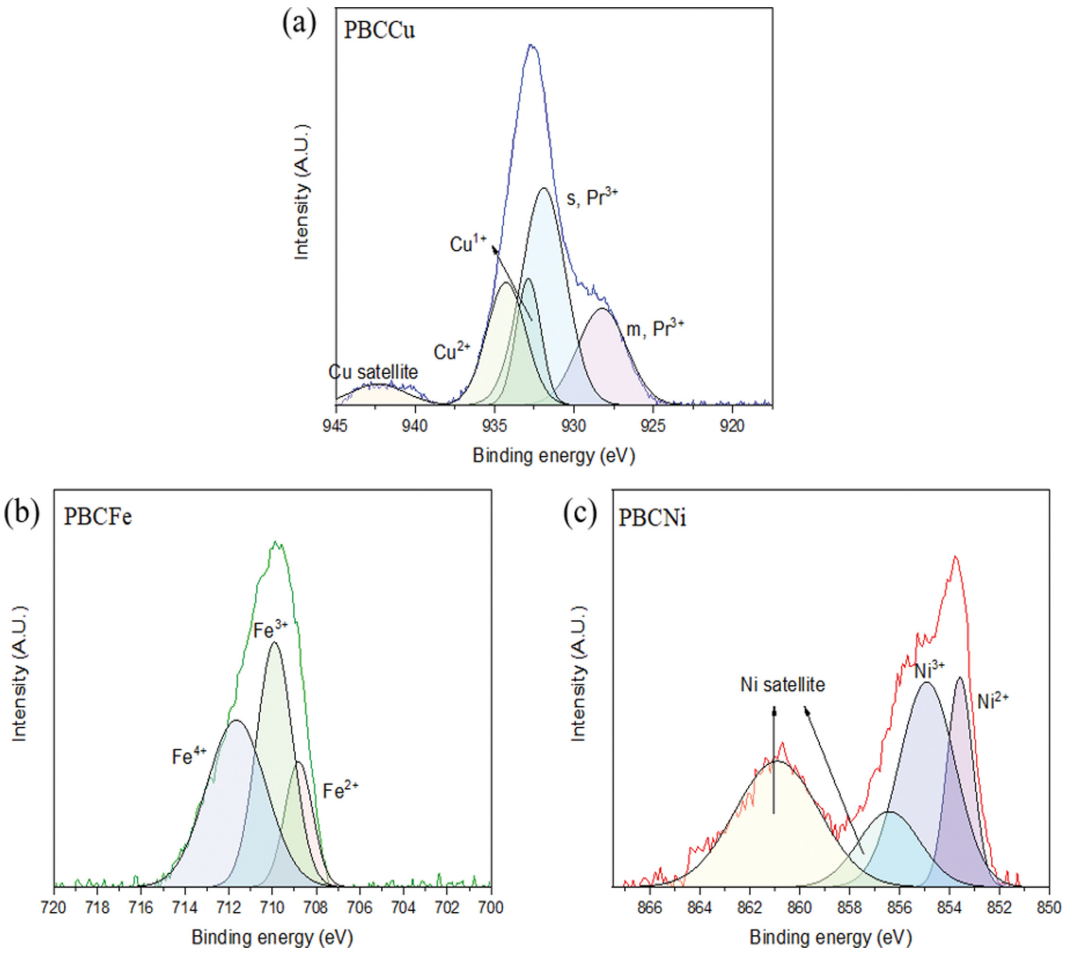

Fig. 4. Core level spectra (solid line) and the fit results (colored area) (a) Pr $3d_{5/2}$ and Cu $2p_{3/2}$ for PBCCu, (b) Fe $2p_{3/2}$ for PBCFe, (c) Ni $2p_{3/2}$ for PBCNi.

Table 2
Co and Me ionic ratio of each elements in $PrBaCoMeO_{5+\delta}$ by the XPS results

Specimen	Peak fitting result (%)							Average oxidation state
	Co			Me (Me = Cu, Fe, Ni)				
	2+	3+	4+	1+	2+	3+	4+	
PBCO	5.39	63.13	31.48	-	-	-	-	3.26
PBCCu	-	64.29	35.71	39.43	60.57	-	-	2.48
PBCFe	1.76	61.29	36.95	-	15.68	39.80	44.52	3.32
PBCNi	1.51	57.29	41.19	-	31.86	68.14	-	3.04

average oxidation number of B site ions from 3.26 (PBCO) to 2.48. In the case of PBCFe, the ratio of Co^{2+} decreases from 5.39% to 1.76%, but the ratio of Co^{4+} also increases from 31.48% to 36.95%, the content of Fe^{4+} becomes 44.52%, and the average oxidation number of B site ions increases to 3.32. In the case of PBCNi, 31.86% of Ni^{2+} is formed and the average oxidation number of B site metal ions decreases to 3.04. But it is difficult to directly explain the generation of oxygen vacancies with the average oxidation number since NiO is formed as confirmed in the XRD results. Therefore, the largest number of oxygen vacancies are generated in PBCCu, and oxygen ion pathways can be generated more efficiently.

Figure 5 shows the structure of the valence band of (Pr, Ba)(Co, Me)$O_{5+\delta}$ (Me = Cu, Fe, Ni). Shallow core level was confirmed in Ba 5p (11~15 eV) and Pr 5p-O 2s bonding (16~21 eV) [24]. The band corresponding to 0~5 eV is composed of transition metal 3d orbitals and O 2p orbital (4.5 eV) and is closely related to the B site

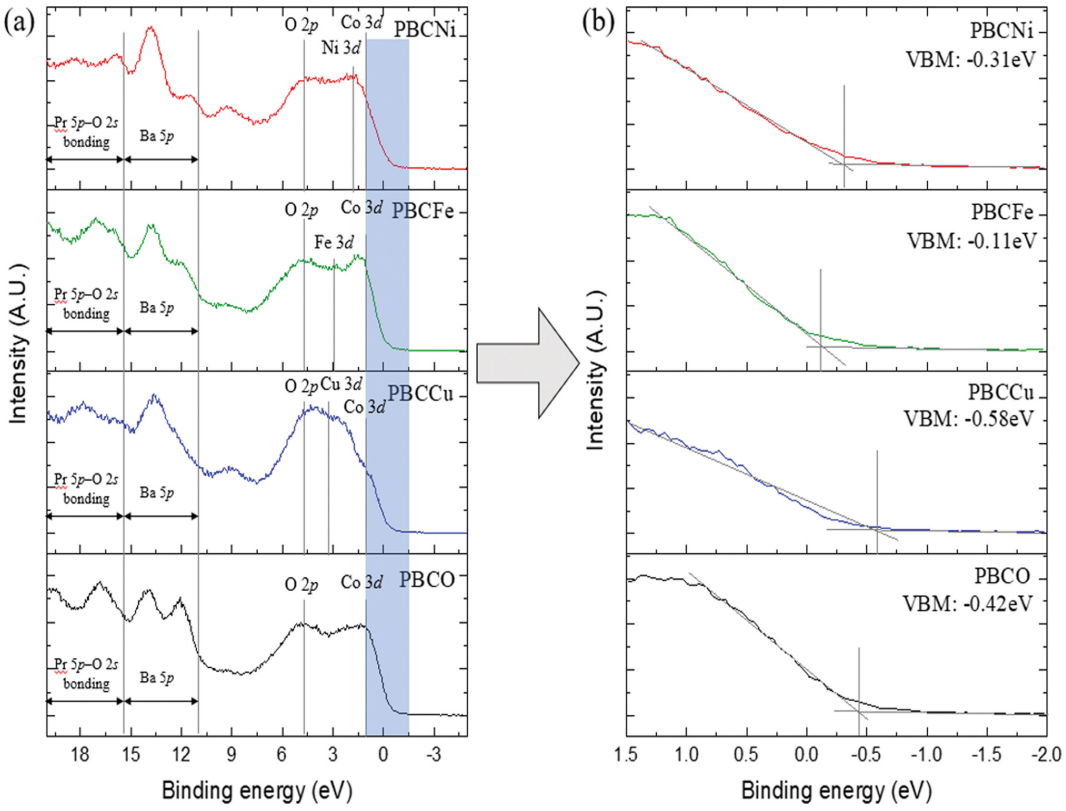

Fig. 5. (a) Valence band (VB) spectra normalized to the integrated intensity and (b) linear fit of the leading edge of the VB used to obtain the valence band maximum (VBM) for PBCMe.

ion [26,27]. The uppermost part of the valence band is composed of the B site metal and oxygen ions and is influenced by them. In addition, the valence band maximum (VBM) is chemically equivalent to HOMO and affects the interaction with oxygen molecules adsorbed on the electrode surface. The higher the VBM, the easier it is to adsorb the diffused oxygen and make the reaction easier [28].

PBCO has a VBM of –0.42 eV by the Co 3d orbital formed at about 1 eV. In the case of PBCCu, a wide energy band is formed by Cu 3d orbital in the 3.1 eV region, and this band forms a VBM of –0.58 eV together with the Co 3d band. PBCFe has a weak energy band at 2.9 eV by Fe 3d orbital, and VBM is –0.11 eV, which is less than PBCO. In the case of PBCNi, an energy band is formed at about 2 eV by Ni 3d orbital, so that VBM becomes –0.31 eV. Through this result, it is considered that PBCCu has the highest VBM and can most easily adsorb and react with oxygen in the air. Considering both VBM and oxidation number of B site ions together, PBCCu formed the most oxygen vacancies and can react most easily with oxygen in the air, so it is expected to have a lower polarization resistance than other compositions.

Figure 6 shows the electrical conductivity of PBCMe.

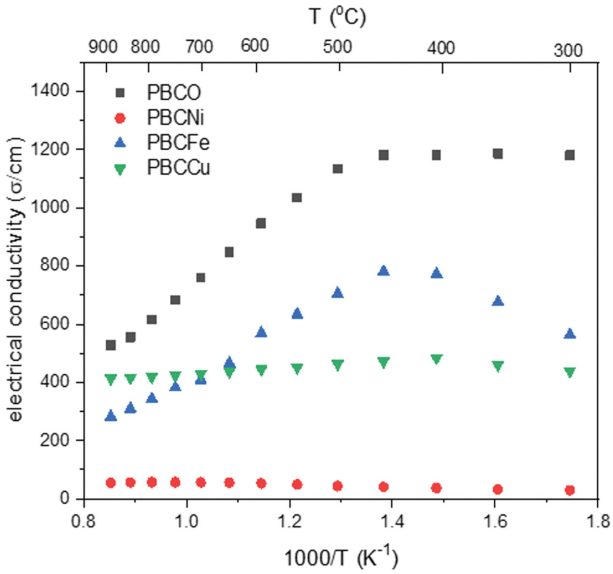

Fig. 6. DC conductivity of PBCMe at 300~900°C.

The electrical electrical conductivity gradually decreases as the temperature increases, this is because the layered perovskite oxides exhibit metallic electrical properties. When other metal ions are substituted for the Co ions of the B site, the electron scattering increases during elec-

tron conduction, and the electrical conductivity decreases in other compositions compared to PBCO [29]. PBCO, PBCFe, and PBCCu are suitable because they show a conductivity of more than 100S/cm, which is a conductivity for using a conductive ceramic material as an electrode [30]. But the electrical conductivity of PBCNi is greatly reduced because of the insulating phase, NiO.

The conductivities of PBCO and PBCFe decreased with increasing temperature, while PBCCu hardly changed. This is because the Co and Fe ions included in PBCO and PBCFe can have an oxidation value of +2 to +4, and the oxidation value is easier to change than that of Cu ion, so that they exhibit metallic conduction characteristics. Carriers are scattered by the lattice and the electrical conductivity decrease with increasing temperature. On the other hand, the PBCCu shows semiconductor like conduction behavior because the oxidation state of Cu ion is not easily changed, so the change in electrical conductivity according to temperature is not large compared to PBCO and PBCFe.

Figure 7 shows the polarization resistance of PBCMe at 600°C. PBCNi showed about 40 times higher polarization resistance (41.67 Ω cm^2) than other phases due to the formation of the NiO insulating phase like the electrical conductivity. PBCO, PBCCu, and PBCFe showed measurement values of 0.91 Ω cm^2, 0.77 Ω cm^2, and 1.06 Ω cm^2, respectively. This can be understood as the relationship between the generation of oxygen vacancies, which act as oxygen absorption site, and the interaction with the adsorbed oxygen. PBCCu shows the lowest B site metal ion oxidation number and the highest VBM of −0.58 eV, showing 0.77 Ω cm^2, which is lower than that of PBCO showing 0.91 Ω cm^2. However, PBCFe differs from its excellent electrical conductivity. Higher B site average oxidation number than PBCO and the lowest VBM of −0.11 eV and shows higher polarization resistance than PBCO.

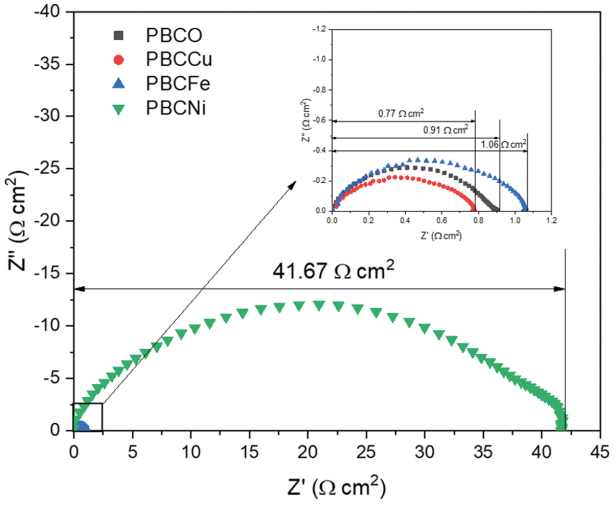

Fig. 7. Nyquist plot of PBCMe in air at 600°C.

4. Conclusion

We studied the electrochemical properties and electronic structures of PBCMe. It was confirmed that PrBaCoCuO$_{5+\delta}$ (PBCCu) and PrBaCoFeO$_{5+\delta}$ (PBCFe) showed Cubic and Orthorhombic structures, respectively, but PrBaCoNiO$_{5+\delta}$ (PBCNi) was not easily doped due to NiO precipitation. PBCCu has an average particle diameter of 1093 nm compared to powders of other compositions, and PBCO and PBCFe each have an average particle diameter of 495.1 nm and 728 nm. The average particle diameter is larger, because Cu doping lowers the melting point during calcination and accelerates the grain growth.

In PBCMe, the average oxidation values of B site ions were found to be 3.26 (PBCO), 2.48 (PBCCu), 3.32 (PBCFe), respectively, and valence band maximum (VBM) was −0.42 eV (PBCO), −0.58 eV (PBCCu), −0.11 eV (PBCFe). It is expected that Cu has the lowest oxidation value and the highest VBM interacts with adsorbed oxygen. Accordingly, the polarization resistance was 0.91 Ω cm^2 (PBCO), 0.77 Ω cm^2 (PBCCu), 1.06 Ω cm^2 (PBCFe) at 600°C, showing the lowest polarization resistance of Cu. The electrical conductivity was 903.99 S/cm in PBCO, 442.33 S/cm in PBCCu, and 530.19 S/cm in PBCFe on average. This implies that when other metal ions are substituted for the Co ions of the B site, the electron scattering increases during electron conduction, and the electrical conductivity decreases in other compositions compared to PBCO. In the case of PBCNi, the average conductivity was 47.83 S/cm, which is believed to be due to the formation of NiO, an insulating phase.

Acknowledgement

This work was supported by a 2-Year Research Grant of Pusan National University.

References

[1] S.P.S. Badwal and K. Foger, “Solid oxide electrolyte

fuel cell review", Ceram. Int. 22 (1996) 257.
[2] M.A. Laguna-Bercero, "Recent advances in high temperature electrolysis using solid oxide fuel cells: A review", J. Power Sources 203 (2012) 4.
[3] N.P. Brandon, S. Skinner and B.C. Steele, "Recent advances in materials for fuel cells", Annu. Rev. Mater. Res. 33 (2003) 183.
[4] A.M. Hussain and E.D. Wachsman, "Liquids-to-power using low-temperature solid oxide fuel cells", Energy Technol. 7 (2019) 20.
[5] S.B. Adler, X.Y. Chen and J.R. Wilson, "Mechanisms and rate laws for oxygen exchange on mixed-conducting oxide surfaces", J. Catal. 245 (2007) 91.
[6] C. Lim, A. Jun, H. Jo, K.M. Ok, J. Shin, Y.W. Ju and G. Kim, "Influence of Ca-doping in layered perovskite $PrBaCo_2O_{5+\delta}$ on the phase transition and cathodic performance of a solid oxide fuel cell", J. Mater. Chem. A 4 (2016) 6479.
[7] Y.F. Sun, Y.Q. Zhang, B. Hua, Y. Behnamian, J. Li, S.H. Cui, J.H. Li and J.L. Luo, "Molybdenum doped $Pr_{0.5}Ba_{0.5}MnO_{3-\delta}$ (Mo-PBMO) double perovskite as a potential solid oxide fuel cell anode material", J. Power Sources 301 (2016) 237.
[8] G. Tsekouras, D. Neagu and J.T. Irvine, "Step-change in high temperature steam electrolysis performance of perovskite oxide cathodes with exsolution of B-site dopants", Energy Environ. Sci. 6 (2013) 256.
[9] L. Jiang, T. Wei and Y. Huang, "Double-perovskite electrode design strategies and research progress for SOFCs", J. Electrochem. Soc. 9 (2022) 064508.
[10] Y.H. Joung, H.I. Kang, W.S. Choi and J.H. Kim, "Investigation of X-ray photoelectron spectroscopy and electrical conductivity properties of the layered perovskite $LnBaCo_2O_{5+\delta}$ (Ln = Pr, Nd, Sm, and Gd) for IT-SOFC", Electron. Mater. Lett. 9 (2013) 463.
[11] R. Strandbakke, "Oxygen electrodes for ceramic fuel cells with proton and oxide ion conducting electrolytes", University of Oslo (2014) 13.
[12] A. Jun, J. Kim, J. Shin and G. Kim, "Perovskite as a cathode material: a review of its role in solid-oxide fuel cell technology", ChemElectroChem 3 (2016) 511.
[13] J. Liu, H. Liu, H. Chen, X. Du, B. Zhang, Z. Hong, S. Sun and W. Wang, "Progress and challenges toward the rational design of oxygen electrocatalysts based on a descriptor approach", Adv. Sci. 7 (2020) 1901614.
[14] A. Grimaud, K.J. May, C.E. Carlton, Y.L. Lee, M. Risch, W.T. Hong, J. Zhou and Y. Shao-Horn, "Double perovskites as a family of highly active catalysts for oxygen evolution in alkaline solution", Nat. Commun. 4 (2013) 1.
[15] Y.L. Lee, J. Kleis, J. Rossmeisl, Y. Shao-Horn and D. Morgan, "Prediction of solid oxide fuel cell cathode activity with first-principles descriptors", Energy Environ. Sci. 4 (2011) 3966.
[16] Z. Zhu, Y. Shi, C. Aruta and N. Yang, "Improving electronic conductivity and oxygen reduction activity in Sr-doped lanthanum cobaltite thin films: cobalt valence state and electronic band structure effects", ACS Appl. Energy Mater. 1 (2018) 5308.
[17] T. Chen, H. Zhao, Z. Xie, L. Feng, X. Lu, W. Ding and F. Li, "Electrical conductivity and oxygen permeability of $Ce_{0.8}Sm_{0.2}O_{2-\delta}$-$PrBaCo_2O_{5+\delta}$ dual-phase composites", Int. J. Hydrogen Energy 37 (2012) 5277.
[18] M. Jana, A. Sil and S. Ray, "Tailoring of surface melting of oxide based catalyst particles by doping to influence the growth of multi-walled carbon nano-structures", Carbon 49 (2011) 5142.
[19] N. Tsvetkov, B.C. Moon, J. Lee an J.K. Kang, "Controlled synthesis of nanocrystalline Nb: $SrTiO_3$ electron transport layers for robust interfaces and stable high photovoltaic energy conversion efficiency in perovskite halide solar cells", ACS Appl. Energy Mater. 3 (2019) 344.
[20] D.S. Bick, J.D. Griesche, T. Schneller, G. Staikov, R. Waser and I. Valov, "$Pr_xBa_{1-x}CoO_3$ oxide electrodes for oxygen evolution reaction in alkaline solutions by chemical solution deposition", J. Electrochem. Soc. 163 (2015) F166.
[21] H.P. Uppara, J.S. Pasuparthy, S. Pradhan, S.K. Singh, N.K. Labhsetwar and H. Dasari, "The comparative experimental investigations of SrMn (Co3+/Co2+) O3±δ and SrMn (Cu2+) O3±δ perovskites towards soot oxidation activity", Mol. Catal. 482 (2020) 110665.
[22] W. Zhang, M. Shiraiwa, N. Wang, T. Ma, K. Fujii, E. Niwa and M. Yashima, "Pr/Ba cation-disordered perovskite $Pr_{2/3}Ba_{1/3}CoO_{3-\delta}$ as a new bifunctional electrocatalyst for oxygen reduction and oxygen evolution reactions", J. Ceram. Soc. Jpn. 126 (2018) 814.
[23] T. Ghodselahi, M.A. Vesaghi, A. Shafiekhani, A. Baghizadeh and M. Lameii, "XPS study of the Cu@Cu2O core-shell nanoparticles", Appl. Surf. Sci. 255 (2008) 2730.
[24] A. Mekki, K.A. Ziq, D. Holland and C.F. McConville, "Magnetic properties of praseodymium ions in Na_2O-Pr_2O_3-SiO_2 glasses", J. Magn. Magn. Mater. 260 (2003) 60.
[25] S.S. Pramana, A. Cavallaro, C. Li, A.D. Handoko, K.W. Chan, R.J. Walker, A. Regoutz, J.S. Herrin, B.S. Yeo, D.J. Payne, J.A. Kilner, M.P. Ryan and S.J. Skinner, "Crystal structure and surface characteristics of Sr-doped $GdBaCo_2O_{6-\delta}$ double perovskites: oxygen evolution reaction and conductivity", J. Mater. Chem. A 6 (2018) 5335.
[26] C. Lohaus, A. Klein and W. Jaegermann, "Limitation of Fermi level shifts by polaron defect states in hematite photoelectrodes", Nat. Commun. 9 (2018) 1.
[27] E. Alves, H.P. Martins, S. Domenech and M. Abbate, "Band structure and cluster model calculations of $LaNiO_3$ compared to photoemission, O 1s X-ray absorption, and optical absorption spectra", Phys. Lett. A 383 (2019) 2952.
[28] Y. Chen, Y. Chen, D. Ding, Y. Ding, Y. Choi, L. Zhang, S. Yoo, D. Chen, B. deGlee, H. Xu, Q. Lu, B. Zhao, G. Vardar, J. Wang, H. Bluhm, E.J. Crumlin, C. Yang, J. Liu, B. Yildiz and M. Liu, "A robust and active hybrid catalyst for facile oxygen reduction in solid oxide fuel cells", Energy Environ. Sci. 10 (2017) 964.
[29] J.H. Kim and A. Manthiram, "Layered $LnBaCo_2O_{5+\delta}$ perovskite cathodes for solid oxide fuel cells: an overview and perspective", J. Mater. Chem. A 3 (2015) 24195.
[30] C. Sun, R. Hui and J. Roller, "Cathode materials for solid oxide fuel cells: a review", J. Solid State Electrochem. 14 (2010) 1125.